PONTIFICIA UNIVERSIDAD CATÓLICA DEL PERÚ

ESCUELA DE POSGRADO

On the optoelectronic properties of sputtered aluminium doped zinc oxide: a critical assessment

Trabajo de investigación para obtener el grado académico de Maestro en Física que presenta:

Luis Alonso Enrique Morán

Asesor:

Prof. Dr. Jorge Andrés Guerra Torres

Lima, 2024

Informe de Similitud

Yo, Jorge Andrés Guerra Torres, docente de la Escuela de Posgrado de la Pontificia Universidad Católica del Perú, asesor de trabajo de investigación de maestría titulada *On the optoelectronic properties of sputtered aluminium doped zinc oxide: a critical assessment*, del autor Luis Alonso Enrique Morán, dejo constancia de lo siguiente:

- El mencionado documento tiene un índice de puntuación de similitud de 16%. Así lo consigna el reporte de similitud emitido por el software *Turnitin* el 23/08/2024.
- He revisado con detalle dicho reporte y la Tesis o Trabajo de investigación, y no se advierte indicios de plagio.
- Las citas a otros autores y sus respectivas referencias cumplen con las pautas académicas.

Lugar y fecha:

Lima, 26/08/2024

Jorge Andrés Guerra Torres	
DNI: 46163725	Firma
ORCID: 0000-0002-1734-6660	

Agradecimientos

Este trabajo, al cual le he dedicado mi mayor esfuerzo durante estos últimos años, representa la conclusión de un proyecto de investigación que involucró el apoyo de diferentes instituciones y personas, a las cuales estoy profundamente agradecido.

En primer lugar, quisiera agradecer el apoyo financiero del Consejo Nacional de Ciencia, Tecnología e Innovación (CONCYTEC) - Programa Nacional de Investigación Científica y Estudios Avanzados (ProCIENCIA) en el marco del concurso "Tesis y Pasantías en Ciencia, Tecnología e Innovación", contrato N°PE501081866-2022-PROCIENCIA. También, junto con el Prof. Dr. Andrés Guerra, agradecemos el apoyo de la *Office Of Naval Research* (ONR), contrato N°N62909-21-1-2034.

Mi inmensa gratitud a mi asesor, el Prof. Dr. Andrés Guerra, por su guía, las oportunidades ofrecidas a lo largo de estos años y su apoyo, tanto académico como profesional. También, agradezco al Dr. Rolf Grieseler y el Prof. Dr. Amaru Töfflinger por ser parte de mi jurado de sustentación de tesis.

Además, me gustaría agradecer al Centro de Caracterización de Materiales (CAM) de la Pontificia Universidad Católica del Perú (PUCP) y al Centro de Investigaciones Tecnológicas, Biomédicas y Medioambientales (CITBM) de la Universidad Nacional Mayor de San Marcos (UNMSM) por brindarme la disponibilidad y el acceso a sus laboratorios y equipamiento con el fin de llevar a cabo esta investigación.

También, quisiera agradecer a todos los miembros del Grupo de Ciencia de los Materiales y Energías Renovables (MatER-PUCP), quienes fueron una pieza clave para el desarrollo de este trabajo y con quienes he compartido experiencias inolvidables. Un agradecimiento especial para Kevin Lizárraga, Erick Serquen, Fabiola Bravo y Alvaro Tejada por la mentoría e ideas brindadas durante mis años en la Maestría en Física.

Resumen

En este trabajo, películas delgadas de óxido de zinc dopado con aluminio (AZO) con diferentes concentraciones de aluminio (Al) fueron crecidas por pulverización catódica de radiofrecuencia y luego fueron calentadas a 400°C en una atmósfera de Argón. El espectro de absorción del óxido de zinc (ZnO) exhibe una contribución de la absorción excitónica a la absorción fundamental que típicamente no es considerada en ZnO dopado con Al. No obstante, se muestra que la banda de excitones libres es aún visible en AZO con bajas concentraciones de Al. Adicionalmente, los estados de defectos, inducidos por el dopaje, incrementan el tamaño de los estados de cola. Estos dos factores, estados de cola y bandas de excitones libres, tienen un efecto substancial en los valores del ancho de banda óptico determinado a partir de la absorción fundamental y deben ser tomados en cuenta con modelos adecuados. En este trabajo, usamos un modelo recientemente desarrollado basado en el modelo de dispersión óptico de Elliot para determinar con precisión el ancho de banda óptico, la energía de ligadura de los excitones y la energía de Urbach de películas delgadas de AZO. Por otro lado, analizamos la absorción de portadores de carga libres, la cual es típicamente modelada por el modelo de dispersión de Drude. Sin embargo, este último no toma en cuenta el hecho de que los centros de dispersión también interactúan con el campo eléctrico externo. Para considerar este efecto, varios modelos han sido propuestos para analizar la resistividad dinámica del material. Típicamente, la resistividad dinámica tiene una dependencia exponencial y un valor de -1.5 es asumido para semiconductores altamente dopados. En este trabajo, dejamos este parámetro libre obteniendo una mejor descripción de los portadores de carga libres y su variación con el dopaje de aluminio.

Contents

List of Figures

On the optoelectronic properties of sputtered aluminium doped zinc oxide: a critical assessment

L. A. Enrique[1,†], S. Mishra[1], E. Serquen[1], F. Bravo[1], K. Lizárraga[1,2], M. Piñeiro[1], P. Llontop[1,3], J. A. Guerra[1,‡]

[1]Departamento de Ciencias, Secci´on F´ısica, Pontificia Universidad Cato´lica del Peru´ (PUCP), 1801 Av. Universitaria, 15088, Lima, Peru´
[2]Instituto de F´ısica, Universidade Federal Fluminense, Rio de Janeiro, Brazil
[3]University of Twente, Inorganic Materials Science Department, 7500 AE Enschede, The Netherlands

E-mail: †luis.enriquem@pucp.edu.pe, ‡guerra.jorgea@pucp.edu.pe

20 September 2024

Abstract. Aluminium doped zinc oxide (AZO) thin films with substrate different aluminium (Al) concentrations were grown by RF-magnetron sputtering with active cooling. The absorption coefficient spectra of zinc oxide (ZnO) exhibits an excitonic absorption contribution to the fundamental absorption that typically is not considered in AZO when determining the optical bandgap. Notwithstanding, here we show that the latter free exciton band remains visible in AZO even at relatively high aluminium concentrations. Additionally, the doping-induced defect states increases the width of tail states. These two factors, tail states and free exciton bands, have a substantial effect on the values of the optical bandgap determined from the fundamental absorption, and thus must be taken into account with adequate models. In this work, we use a recently developed Elliot-based optical dispersion model to accurately determine the optical bandgap, exciton binding energy and Urbach energy of AZO thin films. On the other hand, we assess the infrared free carrier absorption, typically modelled by the Drude dispersion formula, by considering a frequency-dependent dynamical resistivity and the polar nature of the ZnO lattice. Normally, the exponent of the dynamical resistivity power law dependence is assumed as -1.5 for highly doped semiconductors. Notwithstanding, here we let this exponent as a free fitting parameter to assess the effect of distinct scattering mechanisms present in sputtered AZO thin films and its dependence with the Al doping concentration.

20 September 2024

Keywords: AZO, dynamical resistivity, excitons

1. Introduction

Aluminium doped zinc oxide (AZO) is a transparent conductive oxide (TCO) that has been widely used for several applications, such as smart displays [1], solar cells [2] and gas sensors [3]. Nonetheless, a deep understanding of the optoelectronic properties of the material is necessary to tailor and tune the material for optimal performance depending on the use. For instance, the optical window of AZO is affected by its degenerated semiconductor character, induced by the high n-type doping with aluminium (Al) ions and the presence of intrinsic defects, such as zinc interstitials [4] and oxygen vacancies [5]. In the short wavelength region, the fundamental absorption edge is determined by the optical bandgap E_g^{opt}, which is blue shifted due to the well-known Burstein-Moss effect [6]. On the other hand, in the long wavelength region, the plasma edge is influenced by the free carrier absorption, which can have a negative impact on the efficiency of solar cells [7,8]. Therefore, a procedure based on an accurate description of both optical absorption processes is necessary to precisely determine the optoelectronic characteristics of the material.

Typically, the optoelectronic properties of AZO thin films are assessed by modeling the photon energy dependence of the complex dielectric function $\tilde{\varepsilon}(\hbar\omega)$, which can be decomposed in two spectral regions of interest due to the wide bandgap of TCOs [7–10]. The first one is the UV region, in which the fundamental band-to-band transitions take place [11], the second one is the IR region, which is dominated by intra-band electronic transitions [12]. In the UV region, $\tilde{\varepsilon}(\hbar\omega)$ is usually modeled by Tauc-Lorentz oscillators (TL) [13]. However, this optical dispersion model is only suitable for indirect-gap and amorphous materials, thus, the retrieved optical constants have no longer a physical meaning when applied to direct-gap materials. Moreover, the parabolic shape of the TL model does not account for disorder induced states, which have rather an exponential shape [14]. On the other hand, zinc oxide (ZnO) has an excitonic band contribution to the fundamental absorption that remains visible for small Al concentrations [5, 15], which is usually neglected due to the high doping level. Subsequently, E_g is typically obtained from an analogous Tauc formula for direct band-to-band electronic transitions on top of a curve that is intrinsically distinct [14, 16]. The drawback of this procedure is the difficulty in determining the linear region in the analogous Tauc plot due to the presence of tail and possible excitonic states. Then, a considerable bias in the retrieved E_g^{opt} is introduced, which is significant for samples with Urbach energies E_U roughly greater than 60 meV [11, 17] and/or exciton binding energies E_b above 25 meV [18].

In the IR region, the free carrier absorption is usually modeled by the classical Drude model [13], where the complex resistivity $\tilde{\rho}(\omega)$ can be written in terms of the plasma (ω_p) and damping (ω_τ) frequencies, which are related to the $\tilde{\varepsilon}(\omega)$. Nonetheless, this picture does not take into account the interaction between the incoming electric field and charged impurities, which are expected to be present in highly-doped TCOs [9]. The result of considering the latter interaction is that $\tilde{\rho}(\omega)$ the real part of $\tilde{\rho}(\omega)$ obeys a power law behaviour $\rho_1(\omega) \sim \omega^\alpha$ above the plasma frequency [19, 20]. The exponent α is characteristic of the dominant scattering mechanism in the material, where a value of $\alpha = -1.5$ is assumed for point-like ionized impurities [7–9,21]. However, the experimental value of α has been found to range from -1.3 to -2 in sputtered AZO thin films [10]. Furthermore, this assumption neglects the possibility of having competing scattering mechanisms such as ion clusters, among other charged complex defects, which have different characteristic power law exponents [20, 22].

AZO thin films can be grown by different deposition techniques, such as magnetron sputtering [23, 24], pulsed laser deposition [25], atomic layer deposition [26], spin-coating [27] and spray pyrolysis [28]. Among them, magnetron sputtering has the advantage of producing large area homogeneous thin films [29]. The optoelectronic properties of sputtered AZO thin films depend upon the growing conditions [6, 30, 31], the aluminium concentration [32], and can be further modified by post-deposition annealing treatments [33]. However, to the best of our knowledge, there are not reports of sputtered AZO thin films deposited with active substrate cooling ($T_s <$ 25 °C). This growing conditions might be of interest in applications where deposition temperatures above room-temperature can hinder their use [34].

In this work, we assess the optoelectronic properties of AZO thin films grown by radio radio-frequency magnetron sputtering with active substrate cooling. We tailor these properties by varying the doping concentration to induce different charge carrier densities. In the UV spectral region, we determined $\tilde{\varepsilon}(\hbar\omega)$ from a self-consistent [35, 36] approach to avoid any unwanted bias from the assumption of an incorrect dispersion model. We then describe the fundamental absorption edge by a recently developed model that accounts for the contribution of tail and free excitonic states [18]. In the IR spectral region, we probe different extensions of the Drude model for the description of the free carrier absorption [21]. The behaviour of the dynamical resistivity $\tilde{\rho}(\omega)$ and the impact of the power law exponent α value is analyzed. Finally, we assess the relation of the optoelectronic properties of AZO, grown in this fashion, with the aluminium concentration.

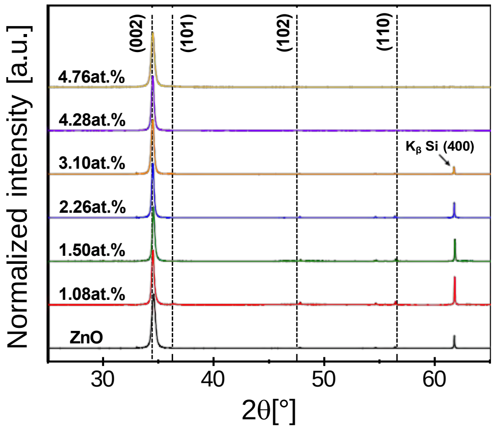

Figure 1: XRD patterns of sputtered AZO thin films grown on n-type silicon (100), after annealing.

2. Experimental details

2.1. Sample preparation

AZO thin films were grown on silicon and two-side polished fused silica substrates by radio-frequency magnetron sputtering using 2 in diameter ZnO and Al targets. The targets were mounted facing the substrate holder at a fixed distance of 6.5 cm. The base pressure of the sputtering chamber was below 2.0×10^{-6} mbar and the working pressure was fixed at 1×10^{-2} mbar. Both targets were sputtered simultaneously under a 30 sccm argon flow. To control the Al concentration, the ZnO RF power was fixed at 80 W while the Al RF power was varied between 12 W and 20 W. During the process, the substrate holder was rotating at 4 rpm to induce an homogeneous deposition and the substrates were actively cooled at 12 °C. An undopped ZnO thin film was grown as a reference sample using the same growing conditions. After deposition, all samples were annealed at 400 °C for 1 h in an Ar atmosphere to enhance their crystallinity. XRD patterns can be found in the supplementary information.

2.2. Elemental composition

Elemental composition was determined from dispersive x-ray spectroscopy using a FEI Quanta 650 scanning electron microscope (SEM). Acceleration voltage was set at 5 keV to avoid the silicon signal contribution from the substrate. Measurements were performed three times in different areas of each sample under a ×400 magnification and then averaged. The quantification was made with the EDAX's TEAM EDS analysis system employing the ZAF correction procedure.

After annealing, we obtained AZO thin films with Al concentrations from 1.08 at.% to 4.76 at.%. Oxygen concentration remains constant for Al concentrations below the reported solubility limit (3–4 at.%) [6, 37], while there is a constant reduction of the Zn concentration for all doping concentrations (Fig. 2a). These results suggest that Al^{3+} ions tend to occupy zinc sites and replace Zn^{2+} in the ZnO structure [38] for Al concentrations below 3 at.%. After this concentration, the further decrease of Zn might be an indirect effect of the segregation of Al atoms at grain boundaries [32, 39] or due to the increase of zinc vacancies V_{Zn} induced by the high Al doping under oxygen rich growing conditions [5]. On the other hand, the small increase of the oxygen concentration might indicate the passivation of oxygen vacancies V_O. Nonetheless, it should be noticed that EDS is less accurate for the elemental quantification of oxygen due to its low characteristic X-ray emission energy [40, 41].

2.3. Structural measurements

X-ray diffraction (XRD) measurements were carried out using a Bruker D8 Focus in Bragg-Bentano (BB) configuration. All samples show a polycrystalline behaviour and are preferentially oriented towards the (002) plane orientation (Fig. 1). Diffraction peaks are consistent with the wurtzite crystal structure of ZnO (PDF 36-1451). The peak around 61.07 °C correspond to the K_β silicon substrate signal [42, 43]. Grain size and microstrain were computed from the (002) peak using a Voigt function single-peak method [44].

Figure 2b depicts the retrieved structural parameters of annealed AZO thin films as a function of the Al concentration. Below the solubility limit, the increase of the grain size might be explained by the increase of the RF applied power [6], having the contrary effect after a certain limit [45]. On the other hand, the increase of the microstrain might indicate the presence of interstitial defects. In particular, oxygen interstitial O_i are expected to be formed at low substrate temperatures [31,46]. Another contribution may be related to the presence of V_{Zn}, which tend to increase the c lattice parameter [5]. After the solubility limit, the variable behaviour of both curves may be explained by variation of the concentration of different defects [47] and/or the formation of secondary phases at the grain boundaries [32]. The latter can not be detected by XRD due to their low amount and very small grains [31]

2.4. Electrical measurements

Resistivity and Hall effect measurements were performed at room temperature using a four probe system in a van der Pauw configuration. The experimental setup system is equipped with a Keithley 6221

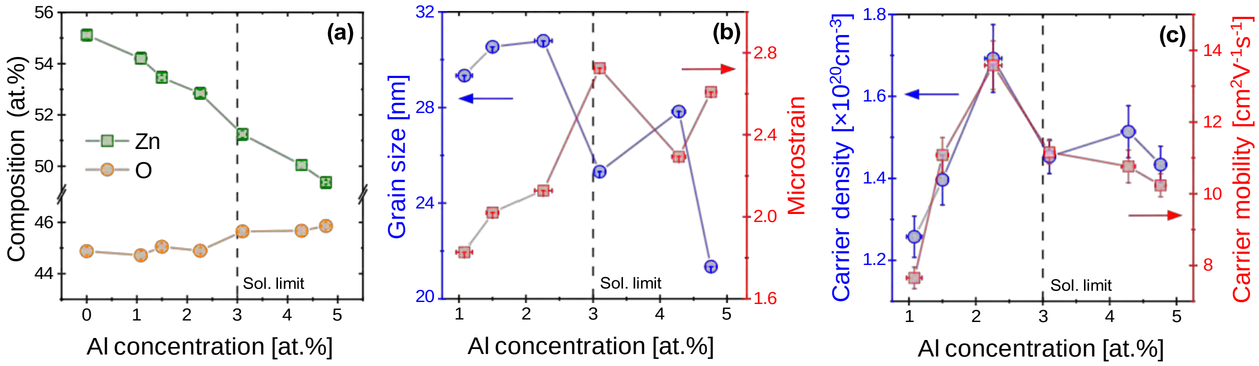

Figure 2: Elemental composition measured by EDS (a), grain size and microstrain retrieved from XRD measurements (b), and Hall effect measured carrier density and mobility (c) of AZO thin films after thermal annealing at 400 °C as a function of the Al concentration. The dotted lines represent the solubility limit of Al in the ZnO structure.

current source, a Keithley 6485 picoammeter and a Keithley 2182A nanovoltemeter. A Keithley 3706A system switch/multimeter together with a 3765 Hall effect card were used for the switching configuration. 40 mm tungsten-rhenium alloy probe tips were used to make electrical contact with the films. Ohmic behavior was checked before each measurement.

Figure 2c shows the Hall carrier density n_e and carrier mobility μ_{Hall} of AZO samples as a function of the doping level, after annealing. For Al concentrations below 3 at.% carrier density increases due the extra charge donated from the replacement of Zn^{2+} ions by Al^{3+} ions. For greater concentrations, n_e is reduced and remains almost constant due to the inclusion of inactive Al ions in the grain boundaries or by the compensation with zinc vacancies V_{Zn} [32]. On the other hand, Hall carrier mobility is expected to decrease with the doping concentration. Nonetheless, the final value of μ_{Hall} is the result of several scattering mechanisms, such as ionized impurities, neutral impurities, cluster scattering and phonon scattering [39]. Then, the initial increasing trend might be related to the enhancement of the grain size in the same concentration range (Fig. 2b) [48, 49] whilst the following decreasing trend could be a consequence of the high defect density induced by the Al doping.

2.5. *Optical measurements*

Optical transmittance and variable angle spectroscopic ellipsometry (VASE) measurements were performed by a SENresearch 4.0 elipsometer in the spectral range from 190 nm to 3500 nm. Ellipsometry measurements were recorded at five incident angles from 50° to 70° in steps of 5°.

The optical model for AZO consisted on a previously characterized substrate layer with a film and roughness layer on top. The latter was include due to the high sensitivity of VASE to even a ~1 nm roughness layer [50]. This layer was modelled by means of the Bruggerman effective medium approximation (EMA), with a fixed air inclusion fraction of 50 % [36, 50–52]. As a first fit, a full spectral range analysis was performed to determine the film and roughness layer thicknesses. Well-known Drude model and Tauc-Lorentz oscillators were used, giving samples thicknesses from 300 nm to 400 nm. The experimental curves were fitted by means of the software SpectraRay/4 from SENTECH Instruments for the thickness determination and the probing of free carrier absorption models, while a Wolfram Mathematica script was used for the self-consistent approach.

3. UV-Vis spectral region

In this section we assess the determination of the complex dielectric function and the description of the fundamental absorption of AZO thin films by means of optical measurements. In this case, the spectral range of interest ranges from 200 nm to 800 nm.

3.1. *Complex dielectric function determination*

The complex dielectric function $\tilde{\varepsilon} = \varepsilon_1 + i\varepsilon_2$ can be calculated from the complex refractive index $\tilde{n}$ since $\tilde{\varepsilon} = (n + ik)^2$, with n the refractive index and k the extinction coefficient, respectively. One way to constrain the solution for $\tilde{\varepsilon}$ is to use several spectral measurements [36]. Here, we use a combination of optical transmittance (T) and spectroscopic ellipsometry (VASE) measurements, the latter being measured at five different angles giving

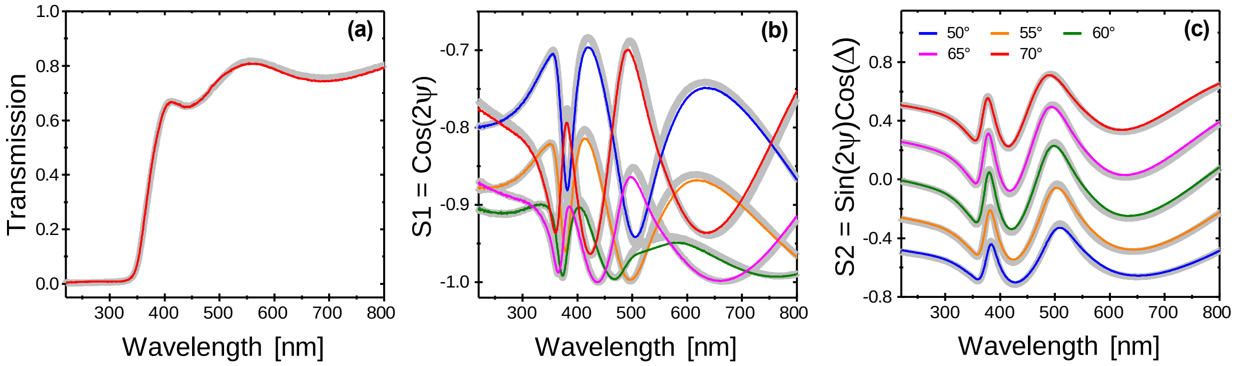

Figure 3: Transmittance T (a) and VASE variables S1 (b) and S2 (c) for the AZO sample with 1.08 at.% aluminium content. Experimental curves (gray) and the corresponding fits (solid lines) with the point-by-point approach are shown.

a total of 11 spectral curves. Another advantage is the complementary information given by each measurement. For instance, T is more sensitive to the bulk properties in transparent regions. Conversely, VASE is very surface sensitive and it offers more information in highly absorbing regions, where T tends to zero and non-meaningful information can be obtained from it [35, 50].

Typically, $\tilde{\varepsilon}(\hbar\omega)$ is determined by assuming an optical dispersion model and directly fitting it to the experimental curves. Nonetheless, this method requires a detailed knowledge of the optical properties of the material to not introduce unwanted artifacts in the retrieved curves. For instance, there are very few dispersion models that account for direct electronic transitions and disorder induced tail states, which are overlapped in the fundamental absorption edge. Recently, new optical models have been developed to properly describe direct-gap semiconductors [14] based on the band-fluctuations approach [11]. However, they are not currently available in commercial softwares. In particular, AZO is a direct-gap material and forcing an incorrect model might induce features that further bias the retrieved optical constants of interest, such as the optical bandgap E_g^{opt}, the Urbach energy E_U and the exciton binding energy E_b.

In this work, instead, we use a self-consistent approach in which the complex refractive index $\tilde{n}$ is determined for each wavelength, i.e. point-by-point. The method consists in taking advantage of redundant spectral curves [35, 36] to minimize the following unbiased estimator:

$$\sigma_i^2 = \left[T_i^{exp} - T_i^{Th}(n_i, k_i, \lambda_i, d_f, d_r)\right]^2 + \sum_{j,k}\left[S_{k,j}^{exp} - S_{k,j}^{th}(n_i, k_i, \lambda_i, \vartheta_j, d_f, d_r)\right]^2 \qquad (1)$$

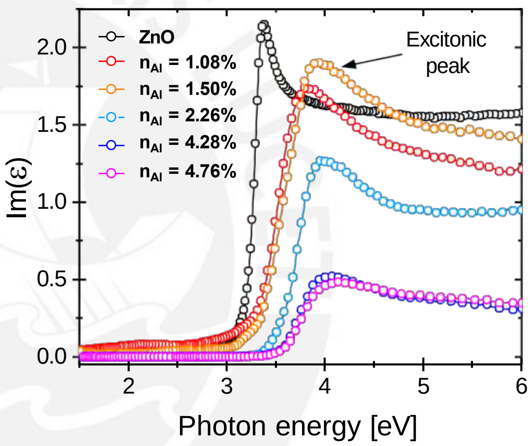

Figure 4: Retrieved imaginary part of the complex dielectric function $\varepsilon_2(\hbar\omega)$ from the point-by-point approach for AZO thin films with different Al concentrations. The presence of the excitonic peak is indicated and the curve of the ZnO reference sample is also shown for comparison purposes.

Here, T is the optical transmittance, S_k are the Stokes parameters related to the VASE measurements and ϑ_j are the incident angles for the ellipsometry measurements. The constants d_f and d_r are the film and roughness layer thicknesses, respectively. The latter thicknesses were previously computed from a full spectral range fit.

Figure 3 depicts the optical transmittance (T) and spectroscopic ellipsometry (VASE) experimental curves for the AZO thin film with 1.08 at.% aluminium content. The optical measurements were fitted using the point-by-point approach with a good agreement with the experimental curves and verified Kramers-

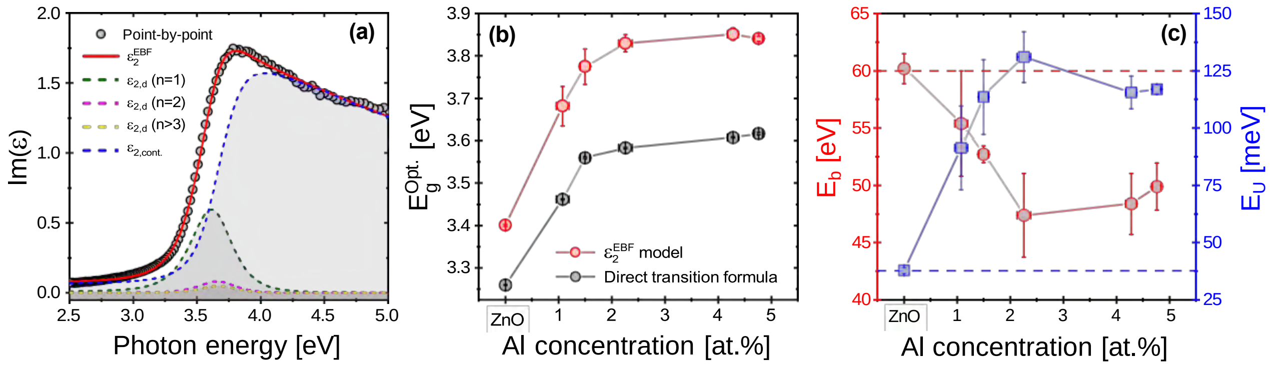

Figure 5: Fit of the EBF_{pV} (solid red line) dispersion model (a), and the retrieved optical bandgap (b), exciton binding energy and Urbach energy (c) as a function of the Al concentration. The continuous and discrete contributions (dashed lines) to the absorption spectra are also shown.

Kronig consistency. Figure 4 shows the retrieved $\varepsilon_2(\hbar\omega)$ curves for the AZO thin films in the UV-Vis spectral region. An increase of the absorption edge with carrier concentration is observed, in agreement with the Burstein-Moss effect.

3.2. Optical constants determination

As it is well established, ZnO is a direct semiconductor with a free exciton band contribution to the fundamental absorption [53]. This feature is observed as a ”shoulder” or excitonic peak in the absorption spectra near the band edge. Therefore, considering the free exciton absorption is crucial to determine the optical bandgap of excitonic materials. This is typically achieved by using an Elliott-based formula to model the absorption edge [12, 54].

In AZO thin films, the aluminium doping increase the charge carrier density of ZnO making it a degenerated semiconductor. Then, it is expected that the exciton binding energy E_b is reduced due to the electrostatic screening of the coulomb interaction between electron-hole pairS [54]. For this reason, the free exciton contribution is usually neglected when fitting the fundamental absorption of heavily-doped semiconductors and E_g is determined by a direct transition formula (Eq. 2) [5, 28, 39, 55]. However, from the retrieved ε_2 curves (Fig. 4), the excitonic contribution seems to still be present even for high Al concentrations. This excitonic feature have also been previously observed in light absorption measurements at low Al concentrations [5, 15]. Additionally, tail states are not commonly considered when attempting to determine the optical bandgap [11, 17].

$$\varepsilon_2 = \frac{A}{\hbar\omega}(\hbar\omega - E_g)^{1/2} \qquad (2)$$

In a recent work, we described the excitonic absorption of GaAs and the family of tri-halide perovskites $MAPbX_3$ (X=Br,I,Cl) [18] by using the band-fluctuations approach [11] and the Sommerfeld enhancement factor. There, the thermal-induced disorder and the uncertainty principle contributions to the broadening of the Elliott formula [56] were taken into account by a band-fluctuations profile ε_2^{BF} and a Lorentzian profile ε_2^{L}, respectively. A pseudo-Voigt profile was used (Eq. 3) leading to an analytical formula with 6 parameters, including E_g^{opt}, E_U and E_b.

$$\varepsilon_2^{EBF}(\hbar\omega) = \eta\varepsilon_2^{BF}(\hbar\omega) + (1-\eta)\varepsilon_2^{L}(\hbar\omega) \qquad (3)$$

A fit using Eq. (3) $\varepsilon_2^{EBF}(\hbar\omega)$ on the imaginary dielectric constant retrieved from the poiny-by-point approach is depicted in Figure 5a for the AZO sample with 1.08 at.%. As shown, the inclusion of the discrete and continuous contributions of the excitonic band, and the disorder induced tail states is necessary to properly reproduce the shape of the absorption edge.

The retrieved optical bandgap from the $\varepsilon_2^{EBF}(\hbar\omega)$ model and the direct transition formula Eq. (2) are compared in Figure 5b. Both approaches show a similar trend versus the doping concentration. However, the direct transition formula tends to underestimate E_g^{opt} by approximately 0.15 eV. The latter owing to the absorption edge shift when neglecting the free exciton band contribution and the Urbach energy (>60 meV).

The trend of E_g can be explained by high doping effects. When Al atoms are introduced in the ZnO structure, they tend to occupy Zn lattice sites. At room temperature, they are expected to be mostly ionized, giving one extra electron to the conduction band. Then, there is an increase of the charge carrier density n_e and, after a critical density, the Fermi level goes into the conduction band and AZO becomes a degenerated semiconductor [57]. Since the conduction band is partially field, direct electronic transitions should occur for energies greater than the E_g of the undoped material, giving rise to the well-known Burstein-Moss shift. Additionally, renormalization effects due to the many-body interactions in both, the conduction and valence band, result a shrinking of the bandgap [9]. Thus, it is expected that E_g^{opt} increases with the aluminum concentration, since there is an increase of the charge carrier density up to the solubility limit. For grater concentrations, E_g^{opt} remains mainly constant in agreement with the behaviour of n_e (Fig. 2c). On the other hand, E_U resembles the trend of the measured microstrain (Fig. 2b). This is expected since the microstrain is directly related with the distortions of the lattice and hence with the internal disorder of the material.

Figure 5c shows the exciton binding energy as a function of the Al concentration. In the case of the ZnO sample, E_b corresponds to the well-known value of 60 meV [53]. For the AZO samples, E_b ranges from 45 meV to 55 meV. This quenching of E_b can be traced to the increase of the electrostatic screening due to the increment of n_e. For this reason, the behaviour of E_b is strongly correlated with the evolution of n_e with the Al concentration (Fig. 2c).

Typically, it is assumed that excitons should not be formed in degenerated semiconductors due to the high free carrier concentration. Mahan [58] studied the excitonic effects in highly-doped semiconductors by treating the conduction band in the high-density limit of the Fermi gas. He predicted an excitonic contribution to the absorption spectra that is further quenched as n_e increases. Recently, Mahan excitons have been reported in methylammonium lead bromide perovskites at room temperature by a combination of ultrafast broadband optical spectroscopy and advanced many-body calculations [59]. Moreover, we should point out that the retrieved values are way above the room-temperature thermal energy 25 meV, indicating that the probability of thermal recombination is low enough to be able to detect them by optical measurements. However, it is possible that the excitonic features are masked in other reports due to the high broadening of the excitonic peak and electrostatic screening effects.

4. IR spectral region

In this section, we describe and evaluate several dispersion theories to account for the free carrier absorption in the spectral range from 800 nm to 3500 nm. The behaviour of the dynamical resistivity and the role of the power law exponent α are assessed.

4.1. *The dynamical resistivity*

The complex dielectric function $\tilde{\varepsilon}(\omega)$ is composed by the contribution of several excitation processes in the material. In particular, for TCOs is possible to isolate the free carrier contribution, which is resonant in the IR spectral range [9]. In this region, the other contributions are constant and $\varepsilon(\omega)$ can be written as follows:

$$\tilde{\varepsilon}(\omega) = \varepsilon_\infty + \tilde{\chi}_{FC}(\omega) \tag{4}$$

Here, $\tilde{\chi}_{FC}$ is the free carrier complex electrical susceptibility and ε_∞ is the sum of the constant contributions from the non-resonant processes in the IR range. If the macroscopic AC fields are described by Maxwell's equations, then is not possible to distinguish between a polarization current $\dot{\mathbf{P}}$ and a current due to free carriers $\mathbf{J}$ [19]. From this argument, we can equate $\tilde{\chi}_{FC}$, and the free carrier contribution can be expressed in terms of a frequency-dependent dynamical resistivity $\tilde{\rho}(\omega) = \rho_1 + i\rho_2$.

$$\tilde{\chi}_{FC}(\omega) = i\frac{\tilde{\sigma}(\omega)}{\varepsilon_0\omega} = \frac{i}{\varepsilon_0\omega\tilde{\rho}(\omega)} \tag{5}$$

In general, the real part ρ_1 of the dynamical resistivity exhibits a bump due to the plasmon resonance near the longitudinal plasma frequency $\omega_p^* \approx \omega_p/\sqrt{\varepsilon_\infty}$, where ω_p corresponds to the plasma frequency in a free electron gas. For $\omega \ll \omega_p^*$, ρ_1 has a constant value, whilst for $\omega \gg \omega_p^*$ it follows a power law $\rho_1 \sim \omega^\alpha$, where α is characteristic of the main scattering mechanism for the free electrons in the material [19, 21]. By combining Eqs. (4) and (5) , the dynamical resistivity can be written in terms of the complex dielectric function:

$$\tilde{\rho}(\omega) = \frac{i}{\varepsilon_0\omega} \cdot \frac{1}{\tilde{\varepsilon}(\omega) - \varepsilon_\infty} \tag{6}$$

Thus, $\tilde{\rho}(\omega)$ can be determined if $\tilde{\varepsilon}(\omega)$ and ε_∞ are known experimentally. In the following sections, we briefly describe how the dynamical resistivity is assessed by different optical dispersion models.

4.2. *The classical Drude model*

The Drude approach is detailed in several textbooks [12, 50] and it is commonly used to describe the free carrier absorption owing to its simplicity and yet good accuracy to retrieve electrical parameters. In this theory, the dynamical resistivity is constant and $\tilde{\varepsilon}(\omega)$ can be written as follows:

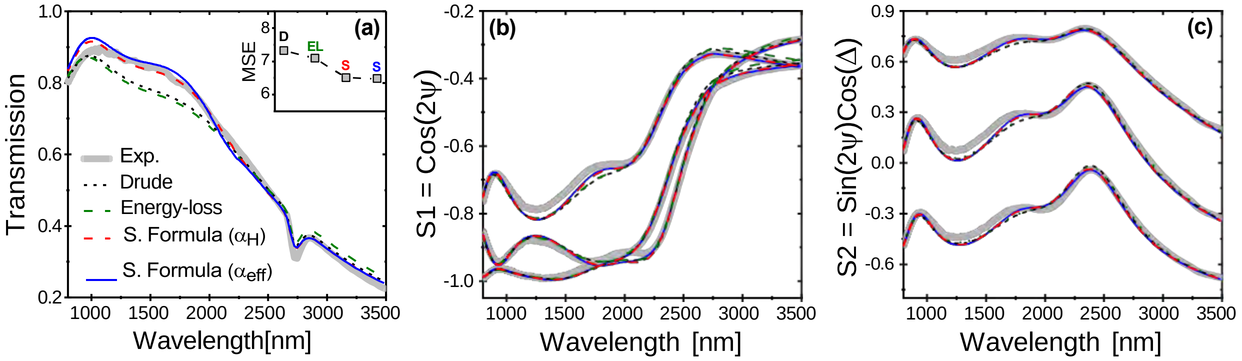

Figure 6: Transmittance (a) and VASE variables S_1 (b) and S_2 (c) in the IR spectral region (800 - 1000 nm) for the AZO sample with 1.08 at.% Al concentration. The fitted curves for the Drude, Energy-loss and Sernelius based formulas are also shown. The latter approach is tested with $\alpha = -1.5$ fixed, S. Formula (α_H), and leaving α as a free parameter, S. Formula (α_{eff}). The inset in (a) corresponds to the mean squared error (MSE) of the fit performed in the SpectraRay/4 software.

$$\tilde{\varepsilon} = \varepsilon_\infty + \frac{i}{\varepsilon_0\omega\left(\rho - \frac{i\omega}{\varepsilon_0\omega_p^2}\right)} \tag{7}$$

with

$$\rho = \frac{\omega_\tau}{\varepsilon_0\omega_p^2}; \quad \omega_p^2 = \frac{n_e e^2}{\varepsilon_0 m_c^*}; \quad \omega_\tau = \frac{e}{\mu m_c^*}$$

Here, ω_p and ω_τ are the plasma and damping frequencies, respectively. This model has just three fitting parameters (ε_∞, ω_p, ω_τ) and has been widely used to describe the free carrier absorption in metals and degenerated semiconductors [50]. Nonetheless, among other effects, this picture does not consider the interaction between the applied electric field and charged scattering centers. The latter interaction has a large contribution in highly doped semiconductors, where the scattering due to ionized impurities is expected to be dominant [9, 10, 21]. The following models are an extension of the Drude formula (Eq. 7) assessing the aforementioned effect yielding to a frequency dependent $\tilde{\rho}(\omega)$.

4.3. The energy-loss method

This method consists on defining two frames of reference (FR), i.e. transport and energy-loss. In the transport FR, the electrons are moving at a constant speed $\mathbf{v}$ and the charged impurities are considered to be fixed. In the energy-loss FR charged impurities are moving with $\mathbf{v}_i = -\mathbf{v}$. Since the energy loss by the impurities is equal to the energy loss by Joule heating in the transport FR, the dynamical resistivity can be isolated and written as [19, 20]:

$$\tilde{\rho}(\omega) = \frac{i n_{sct}}{(2\pi)^3\varepsilon_0 n_e^2 e^2\omega} \times \int_{-\infty}^{\infty} d^3k \frac{k_x^2}{k^2}|\rho_f(k)|^2 \frac{1}{\varepsilon(k,\omega)} - \frac{1}{\varepsilon(0,\omega)} \tag{8}$$

Here, n_{sct} is the density of scatterer centers, n_e is the free charge carrier density, $\rho_f(k)$ is the charge density of the charged impurities and $\varepsilon(k,\omega)$ is the dielectric function of the electron gas. For the case of point-like ionized impurities it has been shown that [9, 20]:

$$\tilde{\rho}(\omega) = \frac{iZ^2 n_i}{6\pi^2\varepsilon_0 n_e^2 e^2\omega} \times \int_0^{\infty} k^2 dk \frac{1}{\varepsilon(k,\omega)} - \frac{1}{\varepsilon(0,\omega)} \tag{9}$$

Here, Z is the charge number and n_i is the density of ionized impurities. In highly doped AZO, ionized impurities are expected to correspond ionized aluminum atoms Al_{Zn} in Zn sites. Thus Z should be fixed at 1, as in the case of ITO [9, 10], leaving a total of 4 fitting parameters (ε_∞, m_c^*, n_e, n_i). For heavily doped semiconductors, the electron gas is treated in the high density limit and $\tilde{\varepsilon}(k,\omega)$ can be modeled by a Lindhard dielectric function i.e. in the random phase approximation (RPA) [20]. Whilst the latter approximation being successful in describing the plasma oscillations, exchange and correlation are not considered. The RPA dielectric function can be improved by a Hubbard correction, which considers exchange, or by the Singwi-Sjölander theory, that accounts for exchange and correlation

[9]. When analyzing the asymptotic behaviour of the dynamical resistivity around ω_p^*, power law exponents of $\alpha_H = -1.5$ and $\alpha_{SS} \approx -2$ are obtained using the Hubbard and Singwi-Sjölander corrections, respectively [9, 10]. It is important to note that this method is more general and can be applied to rather complex scattering centers or time-dependent transport systems, resulting in different characteristic exponents α [20].

4.4. Sernelius based formulas

The polar nature of ZnO has an impact on the dynamical resistivity. The latter effect was studied by Sernelius [60], who applied a strict quantum mechanical formalism to model the contribution of the polar coupling to the dynamical conductivity $\tilde{\sigma}(\omega) = 1/\tilde{\rho}(\omega)$ in heavily doped semiconductors. Due to the complexity, some empirical models that resembles the features of Sernelius' calculation have been proposed [7, 8, 21], where the frequency-dependence of $\tilde{\rho}(\omega)$ is accounted by inserting a frequency-dependent damping frequency $\omega_\tau(\omega)$. In this work, we use a formula based on the one proposed by Pflug [21], which is available in the SpectraRay/4 software:

$$\omega_\tau(\omega) = f(\omega)(\omega_{\tau 0} - \omega_{\tau.ph}(E)) + (1 - f(\omega))(\omega_{\tau 0} + \omega_{\tau 1}) \times \left(\frac{\omega}{\omega_{tr}}\right)^{-\alpha} \tag{10}$$

$$f(\omega) = \frac{1}{1 + \exp\left(\frac{\omega - \omega_{tr}}{\sigma}\right)}$$

Here, $\omega_{\tau.ph}(E)$ accounts for the decrease of $\omega_\tau(\omega)$ due to the electron-phonon interaction, which is modelled by a Gaussian shape. $f(\omega)$ is a sigmoidal function that divides the constant region ($\omega < \omega_{tr}$) from the power law decay region ($\omega > \omega_{tr}$). Therefore, the value of ω_{tr} should be similar to the one of the longitudinal plasma frequency ω_p^* of the material. $\omega_{\tau 1}$ tends to zero during the fitting procedure since it has a competing contribution with $\omega_{\tau 0}$ when describing the power law decay. This can be avoided by implementing an alternative formula proposed by Ruske et al. [7, 8]. Here, $\omega_{\tau 1}$ was fixed at zero, thus having six fitting parameters (ε_∞, ω_p, $\omega_{\tau 0}$, ω_{tr}, σ, α) in total.

Ionized impurities are expected to be the main scattering mechanism in heavily doped semiconductors and an exponent value of $\alpha = -1.5$ is typically assumed [7, 8, 21]. However, α depends on the chosen dielectric function $\varepsilon(k, \omega)$ of the electron gas and it was found to vary experimentally from -1.3 to -2 in AZO thin films [10]. Furthermore, the possibility of having competing scattering mechanisms in materials with a high density of defects is neglected. Therefore, leaving α as a free parameter might lead to a better description of the experimental data. In this case, the retrieved exponent is no longer characteristic of a specific scattering mechanism but rather an effective exponent α_{eff} that accounts for the contribution of different possible scatterer centers in the material.

4.5. IR fitting results

Figure 6 depicts the fit of the IR spectral region using the Drude model, the Energy-loss method and the Sernelius based formulas with $\alpha_H = -1.5$ fixed and with α as a free parameter, i.e. $\alpha = \alpha_{\mathrm{eff}}$. All models have a similar performance when describing the VASE variables S_1 and S_2. On the other hand, the optical transmittance fit has a noticeable improvement when Sernelius based formulas are used, in comparison to the Drude model and the Energy-loss approach. Therefore, considering the polar nature of the ZnO lattice seems to lead to a better description of the experimental data. Nonetheless, there is no apparent impact in the minimized estimator when α is left as an additional fitting parameter.

To assess the role of the power law exponent α we analyze the behaviour of the dynamical resistivity. Jin et al. [10] computed the experimental $\tilde{\rho}(\hbar\omega)$ by means of Eq.(6) for sputtered AZO thin films with unheated substrates. They obtained $\tilde{\varepsilon}(\hbar\omega)$ from optical transmittance T and reflectance R using a matrix formulation of Fresnel's equations and ε_∞ was determined by plotting ε_1 vs $(\hbar\omega)^{-2}$ and extrapolating the linear region towards zero energy, assuming that Drude model applies in this range. Here, we follow a similar procedure by extending the previous point-by-point calculation to compute $\tilde{\varepsilon}(\hbar\omega)$ in the IR spectral region.

Figure 7a shows the real part of the dynamical resistivity $\rho_1(\hbar\omega)$ for the AZO sample with 1.08 at.% Al concentration, the dotted line represents the constant Drude resistivity ($\rho_D \approx 0.96\,\Omega \cdot cm$). When compared to the behaviour predicted by the point-by-point approach, the Sernelius based formulas exhibit a shorter shift in the position of the plasmon resonance. In this case, considering an effective exponent α_{eff} leads to a better description of the features of the plasmon peak and the retrieved exponent is closer to the estimated experimental one.

The estimated power law exponents from the Sernelius based formula (Fig. 7b) are mostly in agreement with the theoretical value estimated for ionized impurities following the Singwi-Sjölander theory ($\alpha_{SS} \approx -2$). Jin et al. found experimental values in the range of $-1.3 < \alpha < -2$. Exponent values greater than -1.5 might be caused by the combined effect of polar coupling $\alpha_{e-ph} = -0.5$ [20]. In our case, the latter is already considered by the $\omega_{\tau.ph}(E)$ term

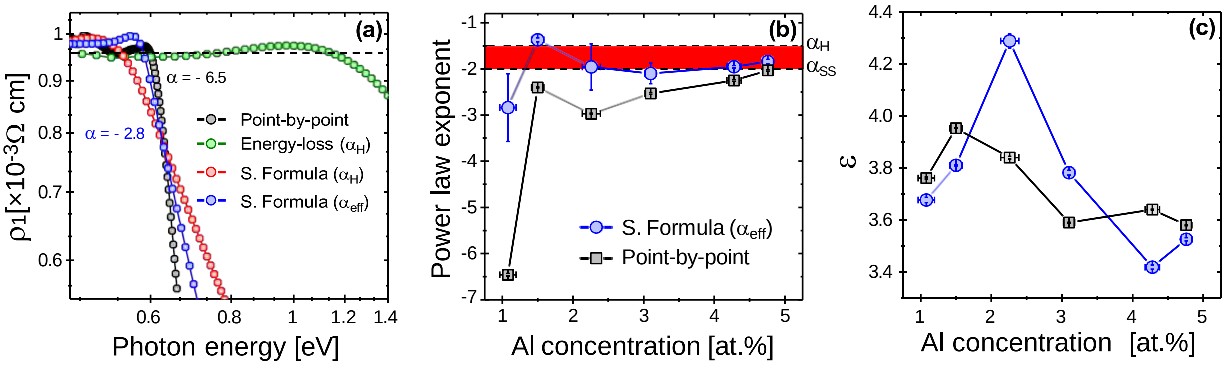

Figure 7: Real part of the dynamical resistivity calculated from the point-by-point approach and the tested free carrier absorption optical models (a). Effective power law exponent α_{eff} (b) and ε_∞ (c) as a function of the Al concentration. α_{eff} values from the point-by-point approach were computed by fitting the linear region of ρ_1 in logarithmic scale.

in Eq. (10).

On the other hand, the point-by-point approach predicts α values lower than α_{SS}, with a lowest value of -6.5 for the AZO grown sample with 1.08 at.% Al. In general, charged impurities become less efficient scatterer centers for $\omega > \omega_p^*$ resulting in a decrease of the resistivity. This effect is enhanced if complex scattering centers are consider, such as, ion clusters [61], monopole lines ($\alpha = -2$) or charged layers ($\alpha = -2.5$) [20]. Thus, the retrieved values suggest the presence of complex defects in our samples. For instance, the presence of oxygen interstitials O_i is expected to be enhanced for sputtered AZO films grown at low substrate temperatures [46], and might form $(Al_{Zn}- O_i)^{-1}$ acceptor-like defects [31]. Menéndez et al. [62] suggested the presence of $(Al_{Zn}- V_{Zn})^{-}$ and $(Al_{Zn} - O_i)^{-1}$ in AZO by contrasting HAXPES measurements with DFT calculations. We believe these defects can account for the low experimental α exponents.

The difference between the exponent values from both approaches might be related to the different behaviour observed in the retrieved ε_∞ values (Fig. 7c). Furthermore, better agreement might be found with other Sernelius based formulas. For instance, Ruske et al. [7] found a better performance by neglecting the $\omega_{\tau.ph}(E)$ term and leaving $\omega_{\tau 1}$ as a free parameter. Nonetheless, it should be noticed that measurement noise might be reflected in the ρ_1 curves from the point-by-point approach which can also affect the retrieved α values.

5. Summary and conclusions

In this work, we have grown aluminium doped zinc oxide (AZO) thin films with different aluminium concentrations and active substrate cooling via magnetron sputtering of a ZnO and Al targets. The optoelectronic properties of AZO were assessed by accurately modeling the complex dielectric function $\tilde{\varepsilon}(\hbar\omega)$ in two spectral regions. For this, we combined optical transmittance and spectroscopic ellipsometry measurements.

In the UV-Vis spectral range, a self-consistent approach revealed the presence of an excitonic band contribution overlapping to the fundamental absorption even for free carriers in the order of 10^{20}cm^{-3}. This feature is in accordance with the presence of Mahan excitons, which were theoretically predicted to affect the light absorption in heavily-doped semiconductors. A recently developed model that accounts for exciton and disorder-induced tail states contribution was used to describe the fundamental absorption. The optical bandgap, Urbach energy and exciton binding energy were retrieve from the fitting of the imaginary part of the dielectric function. Binding energies greater than the room-temperature thermal energy 25 meV and Urbach energies above 60 meV were determined. These values suggest that the previously mentioned contributions should be considered to accurately determine the optical bandgap of AZO thin films.

In the IR spectral range, we probed different dispersion models to describe the free carrier absorption in AZO thin films. The best agreement with the experimental data was achieved when a frequency-dependent dynamical resistivity $\tilde{\rho}(\omega)$ and the polar nature of the ZnO lattice are considered. This was done by using an empirical formula based on the one proposed by Pflug et al. [21]. The real part of $\tilde{\rho}(\omega)$ follows a power law $\rho_1 \sim \omega^{\alpha}$ behaviour for frequencies above the plasma frequency, where α is characteristic for the main scattering mechanisms in the material. Thus, α was left as a free fitting parameter and then compared with the experimental one retrieved from the self-consistency approach. For high Al concentration,

α tends to the characteristic value for ionized impurities considering the Singwi-Sjölander theory. On the other hand, smaller α values for low doping levels might indicate the presence of defect complexes such as $(\mathrm{Al_{Zn}} - \mathrm{V_{Zn}})^{-}$ and $(\mathrm{Al_{Zn}} - \mathrm{O_i})^{-1}$. Nonetheless, further analysis is needed in order to identify the specific contribution from each scattering mechanism in AZO thin films.

The detailed discussion driven in this study is expected to serve as a methodology to precisely determine the optoelectronic properties of heavily doped semiconductors. Particularly, for aluminum doped zinc oxide thin films and ZnO based transparent conductive oxides.

Acknowledgments

This research was supported by CONCYTEC-PROCIENCIA in the framework of the contest E074-2022-01 “Tesis y Pasantías en Ciencia, Tecnología e Innovación grant no. PE501081866-2022-PROCIENCIA and the Office of Naval Research (ONR), grant no. N62909-21-1-2034. The authors acknowledge the Center for Materials Characterization (CAM) at the PUCP and the Center of Technological, Biomedics and Environmental Research (CITBM) at UNMSM for supporting the development of this work.

References

[1] Dimitrov D, Tsai C L, Petrov S, Marinova V, Petrova D, Napoleonov B, Blagoev B, Strijkova V, Hsu K Y and Lin S H 2020 *Coatings* **10** ISSN 2079-6412 URL https://www.mdpi.com/2079-6412/10/6/539

[2] Meza D, Cruz A, Morales-Vilches A B, Korte L and Stannowski B 2019 *Applied Sciences* **9** ISSN 2076-3417 URL https://www.mdpi.com/2076-3417/9/5/862

[3] Kolhe P S, Shinde A B, Kulkarni S, Maiti N, Koinkar P M and Sonawane K M 2018 *Journal of Alloys and Compounds* **748** 6–11 ISSN 0925-8388 URL https://www.sciencedirect.com/science/article/pii/S0925838818309915

[4] Singh C C and Panda E 2018 *Journal of Applied Physics* **123** 165106 ISSN 0021-8979 (*Preprint* https://pubs.aip.org/aip/jap/article-pdf/doi/10.1063/1.5021736/13435149/165106_1_online.pdf) URL https://doi.org/10.1063/1.5021736

[5] Rotella H, Mazel Y, Brochen S, Valla A, Pautrat A, Licitra C, Rochat N, Sabbione C, Rodriguez G and Nolot E 2017 *Journal of Physics D: Applied Physics* **50** 485106 URL https://dx.doi.org/10.1088/1361-6463/aa920b

[6] Misra P, Ganeshan V and Agrawal N 2017 *Journal of Alloys and Compounds* **725** 60–68 ISSN 0925-8388 URL https://www.sciencedirect.com/science/article/pii/S0925838817324866

[7] Ruske F, Pflug A, Sittinger V, Szyszka B, Greiner D and Rech B 2009 *Thin Solid Films* **518** 1289–1293 ISSN 0040-6090 transparent Conductive Oxides URL https://www.sciencedirect.com/science/article/pii/S0040609009007470

[8] Ruske F, Wimmer M, Köppel G, Pflug A and Rech B 2012 Optical characterization of high mobility polycrystalline ZnO:Al films *Oxide-based Materials and Devices III* vol 8263 ed Teherani F H, Look D C and Rogers D J International Society for Optics and Photonics (SPIE) p 826303 URL https://doi.org/10.1117/12.908969

[9] Hamberg I and Granqvist C G 1986 *Journal of Applied Physics* **60** R123–R160 ISSN 0021-8979 (*Preprint* https://pubs.aip.org/aip/jap/article-pdf/60/11/R123/18607609/r123_1_online.pdf) URL https://doi.org/10.1063/1.337534

[10] Jin Z, Hamberg I and Granqvist C G 1988 *Journal of Applied Physics* **64** 5117–5131

[11] Guerra J A, Tejada A, Töfflinger J A, Grieseler R and Korte L 2019 *Journal of Physics D: Applied Physics* **52** 105303 URL https://dx.doi.org/10.1088/1361-6463/aaf963

[12] Yu P Y and Cardona M 2010 *Optical Properties I* (Berlin, Heidelberg: Springer Berlin Heidelberg) pp 243–344 ISBN 978-3-642-00710-1 URL https://doi.org/10.1007/978-3-642-00710-1_6

[13] Volintiru I, Creatore M and Sanden, van de M 2008 *Journal of Applied Physics* **103** 033704–1/10 ISSN 0021-8979

[14] Lizárraga K, Enrique-Morán L A, Tejada A, Piñeiro M, Llontop P, Serquen E, Perez E, Korte L and Guerra J A 2023 *Journal of Physics D: Applied Physics* **56** 365106 URL https://dx.doi.org/10.1088/1361-6463/acd859

[15] Mridha S and Basak D 2007 *Journal of Physics D: Applied Physics* **40** 6902 URL https://dx.doi.org/10.1088/0022-3727/40/22/008

[16] Li Q H, Zhu D, Liu W, Liu Y and Ma X C 2008 *Applied Surface Science* **254** 2922–2926 ISSN 0169-4332 URL https://www.sciencedirect.com/science/article/pii/S0169433207014171

[17] Llontop P, Torres C E, Piñeiro M, Conde L, Tejada A, Töfflinger J A, Rumiche F, Aragón F F H, Pacheco-Salazar D G, Grieseler R, Korte L and Guerra J A 2022 *Journal of Physics D: Applied Physics* **55** 210002 URL https://dx.doi.org/10.1088/1361-6463/ac52fc

[18] Lizárraga K, Llontop P, Enrique-Morán L A, Piñeiro M, Perez E, Serquen E, Tejada A, Ruske F, Korte L and Guerra J A 2023 Description of excitonic absorption using the sommerfeld enhancement factor and band-fluctuations (*Preprint* 2306.17314) URL https://arxiv.org/abs/2306.17314

[19] Gerlach E and Grosse P 1977 *Scattering of free electrons and dynamical conductivity* (Berlin, Heidelberg: Springer Berlin Heidelberg) pp 157–193 ISBN 978-3-540-75358-2 URL https://doi.org/10.1007/BFb0107762

[20] Gerlach E 1986 *Journal of Physics C: Solid State Physics* **19** 4585 URL https://dx.doi.org/10.1088/0022-3719/19/24/004

[21] Pflug A, Sittinger V, Ruske F, Szyszka B and Dittmar G 2004 *Thin Solid Films* **455-456** 201–206 ISSN 0040-6090 the 3rd International Conference on Spectroscopic Ellipsometry URL https://www.sciencedirect.com/science/article/pii/S0040609004000070

[22] Llontop López-Dávalos P D 2023 *Characterization of luminescent ITO:Tb and AZO:Tb thin films prepared by radio frequency magnetron sputtering* Ph.D. thesis Pontificia Universidad Católica del Perú

[23] Minami T, Miyata T, Ohtani Y and Mochizuki Y 2006 *Japanese Journal of Applied Physics* **45** L409 URL https://dx.doi.org/10.1143/JJAP.45.L409

[24] Ruske F, Pflug A, Sittinger V, Werner W, Szyszka B and Christie D 2008 *Thin Solid Films* **516** 4472–4477 ISSN 0040-6090 6th International Conference on Coatings on Glass and Plastics (ICCG6)- Advanced Coatings for Large-Area or High-Volume Products- URL https://www.sciencedirect.com/science/article/pii/S0040609007008978

[25] Agura H, Suzuki A, Matsushita T, Aoki T and Okuda M 2003 *Thin Solid Films* **445** 263–267 ISSN 0040-

6090 proceedings of the 3rd International Symposium on Transparent Oxide Thin films for Electronics and Optics URL https://www.sciencedirect.com/science/article/pii/S0040609003011581

[26] Luka G, Krajewski T A, Witkowski B S, Wisz G, Virt I S, Guziewicz E and Godlewski M 2011 *Journal of Materials Science: Materials in Electronics* **22**

[27] Srinatha N, Raghu P, Mahesh H and Angadi B 2017 *Journal of Alloys and Compounds* **722** 888–895 ISSN 0925-8388 URL https://www.sciencedirect.com/science/article/pii/S0925838817321813

[28] Muiva C, Sathiaraj T and Maabong K 2011 *Ceramics International* **37** 555–560 ISSN 0272-8842 URL https://www.sciencedirect.com/science/article/pii/S0272884210003986

[29] Ellmer K and Welzel T 2012 *Journal of Materials Research* **27** 765–779

[30] Mickan M, Helmersson U and Horwat D 2018 *Surface and Coatings Technology* **347** 245–251 ISSN 0257-8972 URL https://www.sciencedirect.com/science/article/pii/S0257897218304663

[31] Bikowski A, Zajac D A, Vinnichenko M and Ellmer K 2019 *Journal of Applied Physics* **126** 045106 ISSN 0021-8979 (*Preprint* https://pubs.aip.org/aip/jap/article-pdf/doi/10.1063/1.5089555/15232721/045106_1_online.pdf) URL https://doi.org/10.1063/1.5089555

[32] Valenti I, Benedetti S, di Bona A, Lollobrigida V, Perucchi A, Di Pietro P, Lupi S, Valeri S and Torelli P 2015 *Journal of Applied Physics* **118** 165304 ISSN 0021-8979 (*Preprint* https://pubs.aip.org/aip/jap/article-pdf/doi/10.1063/1.4934512/13698684/165304_1_online.pdf) URL https://doi.org/10.1063/1.4934512

[33] Poddar N P and Mukherjee S K 2019 *Journal of Materials Science: Materials in Electronics* **30** 14269–14280 ISSN 1573-482X URL https://doi.org/10.1007/s10854-019-01796-x

[34] Albrecht S, Saliba M, Correa Baena J P, Lang F, Kegelmann L, Mews M, Steier L, Abate A, Rappich J, Korte L, Schlatmann R, Nazeeruddin M K, Hagfeldt A, Grätzel M and Rech B 2016 *Energy Environ. Sci.* **9**(1) 81–88 URL http://dx.doi.org/10.1039/C5EE02965A

[35] Tejada A, Braunger S, Korte L, Albrecht S, Rech B and Guerra J A 2018 *Journal of Applied Physics* **123** 175302 ISSN 0021-8979 (*Preprint* https://pubs.aip.org/aip/jap/article-pdf/doi/10.1063/1.5025728/15213110/175302_1_online.pdf) URL https://doi.org/10.1063/1.5025728

[36] Guerra J A, Tejada A, Korte L, Kegelmann L, Töfflinger J A, Albrecht S, Rech B and Weingärtner R 2017 *Journal of Applied Physics* **121** 173104 ISSN 0021-8979 (*Preprint* https://pubs.aip.org/aip/jap/article-pdf/doi/10.1063/1.4982894/15195367/173104_1_online.pdf) URL https://doi.org/10.1063/1.4982894

[37] Bazzani M, Neroni A, Calzolari A and Catellani A 2011 *Applied Physics Letters* **98** 121907 URL https://api.semanticscholar.org/CorpusID:122258626

[38] Singh A V, Mehra R M, Yoshida A and Wakahara A 2004 *Journal of Applied Physics* **95** 3640–3643 ISSN 0021-8979 (*Preprint* https://pubs.aip.org/aip/jap/article-pdf/95/7/3640/18708422/3640_1_online.pdf) URL https://doi.org/10.1063/1.1667259

[39] Lu J G, Ye Z Z, Zeng Y J, Zhu L P, Wang L, Yuan J, Zhao B H and Liang Q L 2006 *Journal of Applied Physics* **100** 073714 ISSN 0021-8979 (*Preprint* https://pubs.aip.org/aip/jap/article-pdf/doi/10.1063/1.2357638/14972506/073714_1_online.pdf) URL https://doi.org/10.1063/1.2357638

[40] Newbury D E 2012 *Energy Dispersive Spectrometry* (John Wiley Sons, Ltd) pp 1–26 ISBN 9780471266969 (*Preprint* https://onlinelibrary.wiley.com/doi/pdf/10.1002/0471266965.com087.pub2) URL https://onlinelibrary.wiley.com/doi/abs/10.1002/0471266965.com087.pub2

[41] Goldstein J I, Newbury D E, Michael J R, Ritchie N W M, Scott J H J and Joy D C 2018 *Quantitative Analysis: From k-ratio to Composition* (New York, NY: Springer New York) pp 289–307 ISBN 978-1-4939-6676-9 URL https://doi.org/10.1007/978-1-4939-6676-9_19

[42] Gupta A, Paramanik D, Varma S and Jacob C 2004 *Bulletin of Materials Science* **27** 445–451 ISSN 0973-7669 URL https://doi.org/10.1007/BF02708562

[43] Galluzzi A, Buchkov K, Blagoev B S, Paskaleva A, Avramova I, Mehandhziev V, Tzvetkov P, Terziyska P, Kovacheva D and Polichetti M 2023 *Materials* **16** ISSN 1996-1944 URL https://www.mdpi.com/1996-1944/16/19/6547

[44] de Keijser T H, Langford J I, Mittemeijer E J and Vogels A B P 1982 *Journal of Applied Crystallography* **15** 308–314 URL https://doi.org/10.1107/S0021889882012035

[45] Hu Y M, Li J Y, Chen N Y, Chen C Y, Han T C and Yu C C 2017 *Journal of Applied Physics* **121** 085302 ISSN 0021-8979 (*Preprint* https://pubs.aip.org/aip/jap/article-pdf/doi/10.1063/1.4977104/15191699/085302_1_online.pdf) URL https://doi.org/10.1063/1.4977104

[46] Bikowski A, Welzel T and Ellmer K 2013 *Applied Physics Letters* **102** 242106 ISSN 0003-6951 (*Preprint* https://pubs.aip.org/aip/apl/article-pdf/doi/10.1063/1.4811647/14020833/242106_1_online.pdf) URL https://doi.org/10.1063/1.4811647

[47] Sharma B K and Khare N 2010 *Journal of Physics D: Applied Physics* **43** 465402 URL https://dx.doi.org/10.1088/0022-3727/43/46/465402

[48] Zanatta A R and Ferri F A 2014 *Metal-Induced crystallization by homogeneous insertion of metallic species in amorphous semiconductors* cited by: 0 URL https://www.scopus.com/inward/record.uri?eid=2-s2.0-84946740362&partnerID=40&md5=8b46da896c3fe72c37867291df3e5a45

[49] Lermusiaux L, Mazel A, Carretero-Genevrier A, Sanchez C and Drisko G L 2022 *Accounts of Chemical Research* **55** 171–185 ISSN 0001-4842 URL https://doi.org/10.1021/acs.accounts.1c00592

[50] 2007 *Principles of Spectroscopic Ellipsometry* (John Wiley Sons, Ltd) chap 4, pp 81–146 ISBN 9780470060193 (*Preprint* https://onlinelibrary.wiley.com/doi/pdf/10.1002/9780470060193.ch4) URL https://onlinelibrary.wiley.com/doi/abs/10.1002/9780470060193.ch4

[51] Bohórquez C, Bakkali H, Delgado J J, Blanco E, Herrera M and Domínguez M 2022 *ACS Applied Electronic Materials* **4** 925–935 (*Preprint* https://doi.org/10.1021/acsaelm.1c01026) URL https://doi.org/10.1021/acsaelm.1c01026

[52] Ehrmann N and Reineke-Koch R 2010 *Thin Solid Films* **519** 1475–1485 ISSN 0040-6090 URL https://www.sciencedirect.com/science/article/pii/S0040609010014069

[53] Özgür Alivov Y I, Liu C, Teke A, Reshchikov M A, Doğan S, Avrutin V, Cho S J and Morkoç H 2005 *Journal of Applied Physics* **98** 041301 ISSN 0021-8979 (*Preprint* https://pubs.aip.org/aip/jap/article-pdf/doi/10.1063/1.1992666/14961407/041301_1_online.pdf) URL https://doi.org/10.1063/1.1992666

[54] Baranowski M and Plochocka P 2020 *Advanced Energy Materials* **10** 1903659 (*Preprint* https://onlinelibrary.wiley.com/doi/pdf/10.1002/aenm.201903659) URL

https://onlinelibrary.wiley.com/doi/abs/10.1002/aenm.201903659

[55] Li Q H, Zhu D, Liu W, Liu Y and Ma X C 2008 *Applied Surface Science* **254** 2922–2926 ISSN 0169-4332 URL https://www.sciencedirect.com/science/article/pii/S0169433207014171

[56] Elliott R J 1957 *Phys. Rev.* **108**(6) 1384–1389 URL https://link.aps.org/doi/10.1103/PhysRev.108.1384

[57] Ibach H and Lüth H 2009 *"Free" Electrons in Solids* (Berlin, Heidelberg: Springer Berlin Heidelberg) pp 135–158 ISBN 978-3-540-93804-0 URL https://doi.org/10.1007/978-3-540-93804-0_6

[58] Mahan G D 1967 *Phys. Rev.* **163**(3) 612–617 URL https://link.aps.org/doi/10.1103/PhysRev.163.612

[59] Palmieri Tania Baldini E S A A A K M H E F L J F C M 2020 *Nature Communications* **11** 850 ISSN 2041-1723 URL https://doi.org/10.1038/s41467-020-14683-5

[60] Sernelius B E 1987 *Phys. Rev. B* **36**(2) 1080–1089 URL https://link.aps.org/doi/10.1103/PhysRevB.36.1080

[61] Gerlach E and Rautenberg M 1978 *physica status solidi (b)* **86** 479–482 (*Preprint* https://onlinelibrary.wiley.com/doi/pdf/10.1002/pssb.2220860205) URL https://onlinelibrary.wiley.com/doi/abs/10.1002/pssb.2220860205

[62] Menéndez-Proupin E, Palacios P and Wahnón P 2015 *Materials Chemistry and Physics* **160** 420–428 ISSN 0254-0584 URL https://www.sciencedirect.com/science/article/pii/S0254058415300729